



**HAL**  
open science

## Past and future spread of the arbovirus vectors *Aedes aegypti* and *Aedes albopictus*

Moritz U G Kraemer, Robert C. Reiner Jr, Oliver J. Brady, Jane Messina, Marius Gilbert, David M Pigott, Dingdong Yi, Kimberly Johnson, Lucas Earl, Laurie Marczak, et al.

### ► To cite this version:

Moritz U G Kraemer, Robert C. Reiner Jr, Oliver J. Brady, Jane Messina, Marius Gilbert, et al.. Past and future spread of the arbovirus vectors *Aedes aegypti* and *Aedes albopictus*. *Nature Microbiology*, 2019, 13, 10.1038/s41564-019-0376-y . pasteur-02067318

**HAL Id: pasteur-02067318**

**<https://pasteur.hal.science/pasteur-02067318>**

Submitted on 14 Mar 2019

**HAL** is a multi-disciplinary open access archive for the deposit and dissemination of scientific research documents, whether they are published or not. The documents may come from teaching and research institutions in France or abroad, or from public or private research centers.

L'archive ouverte pluridisciplinaire **HAL**, est destinée au dépôt et à la diffusion de documents scientifiques de niveau recherche, publiés ou non, émanant des établissements d'enseignement et de recherche français ou étrangers, des laboratoires publics ou privés.



Distributed under a Creative Commons Attribution 4.0 International License

1 Past and future spread of the arbovirus vectors *Aedes aegypti* and *Aedes*  
2 *albopictus*

3  
4 Kraemer, M.U.G.<sup>1,2,3,§</sup>, Reiner Jr., R.C.<sup>4,§</sup>, Brady, O.J.<sup>5,§</sup>, Messina, J.P.<sup>1,§</sup>, Gilbert, M.<sup>6,7,§</sup>, Pigott, D.M.<sup>4</sup>, Yi,  
5 D.<sup>8</sup>, Johnson, K.<sup>4</sup>, Earl, L.<sup>4</sup>, Marczak, L.B.<sup>4</sup>, Shirude, S.<sup>4</sup>, Davis Weaver, N.<sup>4</sup>, Bisanzio, D.<sup>9</sup>, Perkins,  
6 T.A.<sup>10</sup>, Lai, S.<sup>11,12,13</sup>, Lu, X.<sup>12,13,14,15</sup>, Jones, P.<sup>16</sup>, Coelho, G.E.<sup>17</sup>, Carvalho, R.G.<sup>17</sup>, Van Bortel, W.<sup>18,19</sup>,  
7 Marsboom, C.<sup>20</sup>, Hendrickx, G.<sup>20</sup>, Schaffner, F.<sup>21</sup>, Moore, C.G.<sup>22</sup>, Nax, H.H.<sup>23</sup>, Bengtsson, L.<sup>13,15</sup>, Wetter,  
8 E.<sup>13,24</sup>, Tatem, A.J.<sup>12,13</sup>, Brownstein, J.S.<sup>2,3</sup>, Smith, D.L.<sup>4,25</sup>, Lambrechts, L.<sup>26,27</sup>, Cauchemez, S.<sup>28,29</sup>, Linard,  
9 C.<sup>6,30</sup>, Faria, N.R.<sup>1</sup>, Pybus, O.G.<sup>1</sup>, Scott, T.W.<sup>31</sup>, Liu, Q.<sup>32,33,34,35</sup>, Yu, H.<sup>11</sup>, Wint, G.R.W.<sup>1,36</sup>, Hay, S.I.<sup>4,9,§</sup>,  
10 Golding, N.<sup>37,§</sup>

11 <sup>1</sup>Department of Zoology, University of Oxford, Oxford, UK

12 <sup>2</sup>Harvard Medical School, Harvard University, Boston, USA

13 <sup>3</sup>Boston Children's Hospital, Boston, USA

14 <sup>4</sup>Institute for Health Metrics and Evaluation, University of Washington, WA 98121, USA

15 <sup>5</sup>Centre for Mathematical Modelling of Infectious Diseases, London School of Hygiene and Tropical Medicine,  
16 London, UK

17 <sup>6</sup>Spatial Epidemiology Lab (SpELL), Universite Libre de Bruxelles, B-1050 Brussels, Belgium

18 <sup>7</sup>Fonds National de la Recherche Scientifique, B-1000 Brussels, Belgium

19 <sup>8</sup>Department of Statistics, Harvard University, Cambridge MA, USA

20 <sup>9</sup>Oxford Big Data Institute, Li Ka Shing Centre for Health Information and Discovery, University of Oxford, Oxford,  
21 OX3 7LF, UK

22 <sup>10</sup>Department of Biological Sciences and Eck Institute for Global Health, University of Notre Dame, USA

23 <sup>11</sup>School of Health, Fudan University, Key Laboratory of Public Health Safety, Ministry of Education, Shanghai,  
24 China

25 <sup>12</sup>Department of Geography and Environment, University of Southampton, Southampton, UK

26 <sup>13</sup>Flowminder Foundation, Stockholm, Sweden

27 <sup>14</sup>College of Information System and Management, National University of Defense Technology, Changsha, China

28 <sup>15</sup>Department of Public Health Sciences, Karolinska Institutet, Stockholm, Sweden

29 <sup>16</sup>Waen Associates Ltd, Y Waen, Islaw'r Dref, Dolgellau, Gwynedd LL401TS, UK

30 <sup>17</sup>National Dengue Control Program, Ministry of Health, Brasilia, DF, Brazil

31 <sup>18</sup>European Centre for Disease Prevention and Control, Stockholm, Sweden

32 <sup>19</sup>Institute of Tropical Medicine, Antwerp, Belgium

33 <sup>20</sup>Avia-GIS, Zoersel, Belgium

34 <sup>21</sup>Francis Schaffner Consultancy, Riehen, Switzerland

35 <sup>22</sup>Department of Microbiology, Immunology, and Pathology, Colorado State University, Fort Collins, CO, USA

36 <sup>23</sup>Computational Social Science, ETH Zurich, Zurich, Switzerland

37 <sup>24</sup>Stockholm School of Economics, Stockholm, Sweden

38 <sup>25</sup>Sanaria Institute for Global Health and Tropical Medicine, Rockville, USA

39 <sup>26</sup>Insect-Virus Interactions Group, Department of Genomes and Genetics, Institut Pasteur, Paris 75015, France

40 <sup>27</sup>Centre National de la Recherche Scientifique, Unité de Recherche Associée 3012, Paris 75015, France

41 <sup>28</sup>Mathematical Modelling of Infectious Diseases and Center of Bioinformatics, Biostatistics and Integrative Biology,  
42 Institut Pasteur, Paris, France

43 <sup>29</sup>Centre National de la Recherche Scientifique, URA3012, Paris, France

44 <sup>30</sup>Department of Geography, Universite de Namur, Belgium

45 <sup>31</sup>Department of Entomology and Nematology, University of California, Davis, USA

46 <sup>32</sup>State Key Laboratory for Infectious Disease Prevention and Control, National Institute for Communicable Disease  
47 Control and Prevention, Chinese Center for Disease Control and Prevention, Changping, Beijing 102206, China

48 <sup>33</sup>Collaborative Innovation Center for Diagnosis and Treatment of Infectious Diseases, Hangzhou 310003, China

49 <sup>34</sup>WHO Collaborating Centre for Vector Surveillance and Management, 155 Changbai Road, Changping, Beijing  
50 102206, China

51 <sup>35</sup>Centre for Environment and Population Health, Nathan Campus, Griffith University, 170 Kessels Road,  
52 Queensland 4111, Nathan, QLD, Australia

53 <sup>36</sup>Environmental Research Group Oxford (ERGO), Department of Zoology, Oxford University, Oxford, UK

54 <sup>37</sup>School of BioSciences, University of Melbourne, VIC 3010, Australia

55

56 **Correspondence to:**

57 Moritz U G Kraemer, DPhil

58 Department of Zoology, University of Oxford

59 Oxford, OX13SP, United Kingdom

60 Email: [moritz.kraemer@zoo.ox.ac.uk](mailto:moritz.kraemer@zoo.ox.ac.uk)

61

62 Nick Golding, DPhil

63 School of BioSciences, University of Melbourne

64 VIC 3010, Australia

65 [nick.golding.research@gmail.com](mailto:nick.golding.research@gmail.com)

66

67 Prof. Simon I Hay, DSc

68 Institute for Health Metrics and Evaluation

69 University of Washington,

70 WA 98121, United States

71 [sihay@uw.edu](mailto:sihay@uw.edu)

72

73 <sup>§</sup> Contributed equally to this work as first authors

74

75 [<sup>§</sup>These authors jointly supervised this work](#)

76

77 One Sentence Summary

78 Human mobility patterns and climate changes predict the spread of the arbovirus vectors *Aedes aegypti*  
79 and *Ae. albopictus*, which transmit viruses such as dengue, yellow fever, chikungunya, and Zika.

80 Abstract

81 The global population at risk from mosquito-borne diseases – including dengue, yellow fever,  
82 chikungunya, and Zika – is expanding in concert with changes in the distribution of two key  
83 vectors, *Aedes aegypti* and *Ae. albopictus*. The distribution of these species is largely driven by  
84 both human movement and the presence of suitable climate. Using statistical mapping techniques,  
85 we show that human movement patterns explain the spread of both species in Europe and the  
86 United States of America (USA) following their introduction. We find that the spread of *Ae.*  
87 *aegypti* is characterised by long distance importations, whilst *Ae. albopictus* has expanded more  
88 along the fringes of its current distribution. We describe these processes and predict the future  
89 distributions of both species in response to accelerating urbanisation, connectivity, and climate  
90 change. Global surveillance and control efforts that aim to mitigate the spread of chikungunya,  
91 dengue, yellow fever and Zika viruses must consider the so far unabated spread of these  
92 mosquitos. Our maps and predictions offer an opportunity to strategically target surveillance and  
93 control programs and thereby augment efforts to reduce arbovirus burden in human populations  
94 globally.

95

96 Main text

97 The geographical distributions of the arboviruses dengue, yellow fever, chikungunya, and Zika  
98 have expanded, causing severe disease outbreaks in many urban populations.<sup>1-5</sup> Transmission of

99 these viruses depends, with few exceptions, on the presence of the competent mosquito vectors  
100 *Aedes aegypti* and *Ae. albopictus*<sup>6,7</sup>. Previous predictions of the future distributions of *Aedes*  
101 *aegypti* [= *Stegomyia aegypti*] and *Ae. albopictus* [= *Stegomyia albopicta*] have focussed solely  
102 on climate, despite the known importance of urbanisation and other socioeconomic factors in  
103 defining suitable habitat<sup>8</sup>. Moreover, those projections assumed that both species can fully infest  
104 all areas of predicted newly suitable habitat<sup>4,9</sup>. Recent trends in the global spread of these species,  
105 however, suggest that the process of expansion may be more complex and spatially structured  
106 than previously acknowledged<sup>10</sup>. Expansion from the native ranges in *Ae. aegypti* (from African  
107 forests) and *Ae. albopictus* (from Asia) was precipitated by a shift from zoophily to  
108 anthropophily and by adaptation to container-breeding in domestic or peri-domestic  
109 environments<sup>11,12</sup>. Whilst their short flight ranges limit self-powered dispersal<sup>13</sup>. A century of  
110 rapid human population growth and international trade has enabled their global spread. Trade in  
111 items that provide potential larval development habitats such as tires and potted plants led to  
112 inter-continental dissemination of their desiccation-resistant eggs<sup>14-16</sup>. Moreover, the  
113 establishment of *Ae. albopictus* in locations with cooler climates has been aided by its ecological  
114 plasticity, with eggs able to undergo diapause (dormancy) as one possible explanation for  
115 populations persisting through winters too cold for adult survival<sup>17,18</sup>.

116 Whilst the various routes of inter-continental importation are well described<sup>11,19</sup>, the processes  
117 underlying intra-continental spread of the species remain poorly quantified, preventing informed  
118 prediction of future distributions. Modelling of human-mediated range expansion suggests that  
119 quantitative models of human movement could, and should, be used to predict intra-continental  
120 spread<sup>20-22</sup>. To address this, we developed predictive models of *Ae. aegypti* and *Ae. albopictus*  
121 spread and combined these with forecasts of future climatic conditions and urban growth, to

122 predict the ranges of these medically important vectors from 2015 to 2080 (Extended Data Fig.  
123 1).

124 We collated spatially- and temporally-explicit data on the distributions of *Ae. aegypti* and *Ae.*  
125 *albopictus* and their spread over time in the USA, and *Ae. albopictus* in Europe (Fig. 1, Extended  
126 Data Figs. 2, 3). Extending a previous study<sup>4</sup>, we first mapped contemporary habitat suitability  
127 for each species together with projected suitability in 2020, 2050, and 2080, under three different  
128 Representative Concentration Pathway (RCP) and 17 global climate models (GCMs), as well as  
129 under projections of urban growth. We then parameterised quantitative models of human  
130 mobility using census data on migration and commuting patterns<sup>23,24</sup>, and general movement  
131 patterns derived from mobile phone logs (call detail records) (Extended Data Fig. 1)<sup>23-25</sup>. The  
132 combined predictions from these different mobility models and datasets capture different aspects  
133 of human travel and trade, and their ability to spread *Aedes* eggs and juveniles at different spatial  
134 scales.

135 We tabulated annualised presence records which documented the first detection of each species  
136 in 1,567 different locations over 38 years in Europe (225 / 1,588 districts, between 1979 - 2016)  
137 and 32 years in the USA (1,342 / 3,134 counties, between 1985 and 2016) (Extended Data Fig.  
138 2a, b, c). These data were used to parameterise statistical models of spatial spread for each  
139 species. Detection within a given area was modelled as a function of i) the receptivity of the area  
140 (as determined by the habitat suitability models), ii) long-distance importation pressure (from  
141 multiple human movement models) and iii) short-distance importation pressure from adjacent  
142 areas (to represent natural dispersal). Forward simulation of these fitted models of spatial spread  
143 was then used to predict the future spread or recession of each species, considering climate  
144 changes, urbanisation, and human-mediated importation. To account for potentially biased

145 sampling procedures we performed a comprehensive sensitivity analysis assuming different  
146 levels of detection for both species (Supplementary Information).

147 Short-range importation between adjacent districts played a greater role in the inferred spread  
148 process for *Ae. albopictus* (Fig. 1a, c, d, f) than for *Ae. aegypti* (Fig. 1b, e), which was more  
149 frequently imported over longer distances. Historically, most of the observed range expansion of  
150 *Ae. aegypti* in the USA originated from southern States (Fig. 1b, Extended Data Fig. 2b). Using  
151 thin plate spline regression, we estimated the localised invasion velocity of *Ae. aegypti* spread in  
152 the USA to be relatively homogeneous at ~250km per year (Fig. 1b, e). *Aedes albopictus* spread  
153 in the USA was fastest between 1990 and 1995 (Fig. 1a, d) and has since slowed to about ~60km  
154 per year. In contrast, the estimated rate of spread of *Ae. albopictus* in Europe is faster (~100km  
155 per year) rising to ~150km per year over the last five years (Fig. 1c, f, Extended Data Fig. 2c, f,  
156 i). The geographic origin of recent *Ae. albopictus* spread in Europe seems to be Italy, with the  
157 Alps serving as a dispersal barrier that lowers rates of spread (Extended Data Fig. 2c, f). Once  
158 that barrier has been overcome, however, spread rates beyond the Alps are as high as in Italy.  
159 This may explain the increased rate of spread in recent years, which also corresponds to the  
160 detection of *Ae. albopictus* in areas north of the Alps (Extended Data Fig. 2c, f).

161 Using human-mobility-driven statistical models we can predict the past spread of both mosquito  
162 species with high reliability (Extended Data Fig. 6) and accuracy (out of sample area under the  
163 receiver operating characteristic curve [AUC]: 0.7-0.9, Extended Data Fig. 7). Only slight  
164 improvements are observed when including human mobility models over models that only  
165 included distance and adjacency metrics (Supplementary Information, Extended Data Fig. 12).

166 Further, we evaluated our models' ability to predict the range expansion in Europe using a model  
167 fitted to US data (1,149 records) only. This test similarly documented a high degree of predictive

168 ability (out of sample AUC: 0.8-0.9, Extended Data Fig. 8). In addition, country borders seem  
169 not to limit the spread of the mosquitoes (Extended Data Fig. 11) and our spread model is robust  
170 even under different assumptions in mosquito sampling strategies but the underlying  
171 observational data may impact our estimates of velocity of spread (Supplementary Information).  
172 In contrast, the model fitted to only European data was unable to predict the spread in the USA,  
173 presumably because of the relatively few *Ae. albopictus* records in Europe compared to the USA  
174 (192 records). Therefore we used the model fitted to USA data to project the range of both  
175 species into the future (Supplementary Information). Both *Ae. aegypti* and *Ae. albopictus* are  
176 anticipated to continue expanding beyond their current distributions (Extended Data Figs. 4, 5).  
177 For *Ae. aegypti*, predicted future spread is mostly concentrated within its tropical range and in  
178 new temperate areas in the USA and China; reaching as far north as Chicago and Shanghai by  
179 2050 (Figs. 2, 4, Extended Data Fig. 4). At the expansion front in the United States, our model  
180 predicts the spread to occur mostly through long-distance introductions in large urban areas (Figs.  
181 2a, b, Extended Data Fig. 10). Even under the most extreme scenarios (RCP8.5 in 2080), *Ae.*  
182 *aegypti* is predicted to establish in Europe in only a few isolated regions of southern Italy and  
183 Turkey (Extended Data Fig. 4). By 2080 we predict there will be 159 countries worldwide (range  
184 156 – 162) reporting this species, of which three (range 0-6) will be reporting it for the first time  
185 (Extended Data Tab. 8).

186 By contrast, *Ae. albopictus* is expected to spread broadly through Europe, ultimately reaching  
187 wide areas of France and Germany (Fig. 3b). Areas in northern USA and highland regions of  
188 South America and East Africa are also projected to see establishment of *Ae. albopictus* over the  
189 next 30 years (Figs. 2, 4). At the same time, some areas are predicted to become less suitable for  
190 the species, particularly locations in central southern USA (Fig. 2, Extended Data Fig. 5) and

191 Eastern Europe (Fig. 3) where climate models indicate aridity will increase. Due to *Ae.*  
192 *albopictus* broader distribution in northern latitudes, as in the USA, the spread pressure follows a  
193 clear front-like expansion (Figs. 2c, d). In total, 197 countries (range 181-209) are expected to  
194 report *Ae. albopictus* by 2080, 20 (range 4-32) of those countries will be reporting its presence  
195 for the first time (Extended Data Tab. 8).

196 Spread of both species over the next 5-15 years is predicted to occur independently of extensive  
197 environmental changes as both species continue to expand into their anthropogenic ecological  
198 niches through spatial dispersal. *Aedes albopictus* is anticipated to saturate its ecological niche  
199 between 2030 and 2050 (Figs. 4d, f), and *Ae. aegypti* by 2020 (Figs. 4a,c). Beyond these dates  
200 the predicted expansion of these species will be driven primarily by environmental changes that  
201 create new habitat, including changes in climate, especially temperature (Extended Data Tab. 1,  
202 2), as well as exploitation of the increased availability of large human urban environments. Thus  
203 efforts to curb or reverse climate change are predicted to be insufficient to prevent fully the  
204 expansion of these vector species; significantly greater expansion, however, is predicted,  
205 especially between 2050 and 2080, if emissions are not reduced (Fig. 4). At the same time, future  
206 human population growth is expected to be concentrated disproportionately within areas where  
207 *Ae. aegypti* and *Ae. albopictus* already will be established, leading to large increases in the global  
208 population at risk of diseases transmitted by these species.

209 Overall our predicted expansions will see *Ae. aegypti* invading an estimated 19.96 million km<sup>2</sup>  
210 by 2050 (19.91 – 23.45 million km<sup>2</sup>, depending on the climate and urbanisation scenarios),  
211 placing an estimated 49.13% (48.23 – 58.10%) of the world's population at risk of arbovirus  
212 transmission (Figs. 4c, f).

213 Few countries conduct routine, systematic surveillance for *Ae. aegypti* and *Ae. albopictus*.  
214 Consequently our analysis relies on datasets from the USA and Europe that contain spatio-  
215 temporal biases in reporting (Extended Data Fig. 2), with an implicit assumption that the  
216 processes driving spread in these regions apply elsewhere. These regions have (i) a  
217 comparatively high capacity to track establishment and mitigate the spread of these species and  
218 (ii) openly available datasets on human movement<sup>26</sup>. Our modeled rate of spread is thus most  
219 likely to be biased towards an underestimate of the global rate of spread (Supplementary  
220 Information). We did not model potential changes in human mobility which could increase the  
221 rate of spread of both species as population mobility increases. Competitive displacement may  
222 occur between these two species but this possibility could not be included in this analysis due to  
223 a lack of available data<sup>27,28</sup>. However, current ecological literature and ecological theory suggests  
224 interspecific competition occurs primarily at localized spatial scales and has not been found to  
225 influence species' distributions at a coarser spatial resolution, such as the scale we consider  
226 here<sup>29-31</sup>. As both species are already established on every human-inhabited continent on the  
227 planet, we did not model spread between continents.

228 In the context of predicting mosquito-borne viral transmission, *Aedes* distribution maps have  
229 already been shown to help predict the local<sup>32</sup>, regional<sup>33,34</sup>, and international<sup>1,2,6,7,35,36</sup> spread of  
230 chikungunya, dengue, yellow fever and Zika viruses. Moreover, local outbreaks of these  
231 arboviruses have typically followed within 5-15 years of infestation by *Ae. aegypti* and *Ae.*  
232 *albopictus*, emphasising the importance of vector spread importation as a key risk factor for  
233 arbovirus transmission.

234 There is significant uncertainty surrounding future predictions of changes in climatic conditions.  
235 We used an ensemble approach to propagate the uncertainty from climate scenarios through our  
236 predictions of both *Aedes* species (Figs. 2, 3, 4, Extended Data Figs. 4, 5).

237 Even under current climate conditions and population densities, both vector species will continue  
238 to spread globally over the coming decades, filling unoccupied suitable habitats and posing a risk  
239 to human health in the majority of locations where they survive and reproduce. Thus efforts to  
240 prevent their global dissemination in the near future will be most effective if focussed on  
241 preventing human-mediated spread and establishment. To prevent introductions, countries  
242 should strengthen entomological surveillance, particularly around high-risk introduction routes  
243 such as ports and highways and develop rapid response protocols for vector control to prevent  
244 introduced mosquitoes from establishing permanent populations<sup>37-41</sup>. We expect such efforts will  
245 need to intensify over time as human populations become ever more connected and urban  
246 agglomerations grow further<sup>9</sup>.

247 Beyond 2030 and especially 2050, the distributions of both species will continue to expand, co-  
248 inciding with niche expansion into climatically suitable urban areas as opposed to the exploration  
249 of the current niche. Increased urbanisation worldwide has already put great strains on our ability  
250 to prevent the spread of certain disease vectors and has intensified endemic transmission of  
251 arboviruses<sup>42</sup>. Some areas may become less suitable for human habitation due to climate change  
252 impacts, reducing the number of people living in areas at risk. In the longer term, reducing  
253 emission of greenhouse gases would be desirable to limit the increase in *Ae. aegypti* and *Ae.*  
254 *albopictus* suitable habitat. Every effort must be made to limit factors that contribute to the  
255 global spread of *Ae. aegypti* and *Ae. albopictus* if we are to limit the future burden of the diseases  
256 vectored by these mosquitoes.

257

258

## 259 Methods

260 We used a combination of two approaches to estimate the predicted future distribution of *Ae.*  
261 *aegypti* and *Ae. albopictus*: (1) projecting the environmental suitability of both species using a  
262 set of seven environmental covariates and (2) simulating the spread within each continent using  
263 the species' past dispersal patterns, human movement data, and between region adjacency  
264 matrices (Extended Data Fig. 1). Here we describe the models and data sources for both  
265 processes.

### 266 1. Data

#### 267 1.1. Global mosquito occurrence data

268 We used a previously collated database of 19,930 and 22,137 geositioned occurrence records  
269 for *Ae. aegypti* and *Ae. albopictus* respectively (Extended Data Fig. 3)<sup>43</sup>. Each of these records  
270 corresponds to a unique detection of a mosquito population in a given location at a given point in  
271 time, as described in detail elsewhere<sup>43</sup>. We excluded records that were classified as temporary  
272 presence when such information was available.

#### 273 1.2. Environmental and socio-economic covariates

274 *Aedes* survival is influenced by a variety of climatic and environmental factors such as long term  
275 and inter-annual temperature<sup>44,45</sup>, water availability (described as relative humidity and  
276 precipitation), and degree of urbanisation. We used projections from the “Representative  
277 Concentration Pathways” (RCP) developed by the Intergovernmental Panel on Climate Change  
278 (IPCC)<sup>46</sup> which represent different assumptions about emission scenarios that might result in a  
279 variety of climatic changes over the next 65 years. Here we use RCPs 4.5, 6.0 and 8.5, which

280 assume emission peaks around 2040, 2080 and increases throughout the 21<sup>st</sup> century  
281 respectively<sup>46</sup>. These time points were chosen because (i) 2020 represents the date when the  
282 climate mitigating policies of the Paris Agreement within the United Nations Framework  
283 Convention on Climate Change (UNFCCC) will come into action<sup>47</sup>, (ii) 2080 corresponds to the  
284 date of the emission peaks modelled according to the RCP 6.0 scenario and (iii) 2050 represents  
285 the midpoint between these dates. We use an ensemble of 17 GCMs and pattern scaling to  
286 produce monthly mean values of maximum and minimum temperature and monthly totals of  
287 rainfall as used in MarkSim. Humidity data were calculated from temperature estimates (see  
288 details in section 3). To complement the changes in temperature, relative humidity, and  
289 precipitation, we modelled a continued process of global urbanisation until 2080 using a  
290 probabilistic machine learning algorithm based on Linard et al<sup>48</sup>. Here we use urban growth rates  
291 projected by the United Nations as a predictor variable<sup>49</sup> as well as a range of other critical  
292 covariates, as described in van Vuuren et al<sup>48</sup>.

### 293 1.3. Mosquito spatial spread data

294 A unique set of time-series occurrence records for both species were abstracted from Kraemer et  
295 al.<sup>4,43</sup>, and updated with records obtained from Hahn et al<sup>50</sup>. Records were available for *Ae.*  
296 *aegypti* in the United States from 1995 – 2016 with United States county-specific information  
297 regarding whether the species was present or absent; for *Ae. albopictus* information was  
298 available from the United States (1987 – 2013) and from Europe (1979 -2017) (Fig. 1, Extended  
299 Data Fig. 2). We considered these time periods because they show consistent expansion of the  
300 species distribution as described in Hahn et al<sup>50</sup>.

301 For the United States, counties were identified as reporting presence of either species in a given  
302 year if at least one specimen of any life stage of the mosquito was collected, using any collection

303 method<sup>50</sup>. Sampling efforts, techniques and temporal resolution were heterogeneous across  
304 counties and states in the United States. Therefore, the baseline presence datasets may classify  
305 some areas as absent where either of the two *Aedes* species considered may be present.

306 For Europe, Administrative/Statistical units (NUTS3) were identified as reporting establishment  
307 of either species in a given year if immature stages and overwintering were observed, using any  
308 collection method. Sampling efforts, techniques, and temporal resolution were heterogeneous  
309 across countries and either species may have been absent before investigations were triggered by  
310 citizen complaint. Therefore, dates correspond to published reports or expert-shared data  
311 (VBORNET, VectorNet), and a species could have established earlier in some locations where  
312 regular surveillance had not been implemented. Because we were not able to quantify the  
313 sampling biases, we instead employed a sensitivity analysis to account for potential under- or  
314 over-reporting (see section 2.4).

#### 315 1.4. Human mobility datasets

316 Overland human movements are known to drive the importation of both species<sup>38,39,41</sup>. Therefore  
317 we used human movement data to infer the connectivity between regions as a proxy for  
318 importation risk of *Ae. aegypti* and *Ae. albopictus*.

319 *US commuting data:* For the United States, where both species have been spreading successfully,  
320 we obtained data on workforce commuting flows from county to county between 2009 – 2013,  
321 conducted by the American Community Survey (ACS). Data are freely available at  
322 <http://www.census.gov/hhes/commuting/>. Here, commuting was defined as a worker’s travel  
323 between home and workplace, where the latter refers to the geographical location of the worker’s  
324 job. Daytime population refers to the estimated number of people who are residing and working  
325 in an area during “daytime working hours”. The data represent 3,134 counties including 50 states

326 and the District of Columbia (DC) but excluding Puerto Rico. The generalisability of this data  
327 has been demonstrated in studies that have successfully approximated human movements  
328 derived from mobile phone data and predicted the spread of infectious diseases<sup>24</sup>. As described  
329 below in section 2.3 in detail, we considered gravity and radiation movement models as well as  
330 nearest neighbour-type movements for human movement. We used the fitted models from the  
331 USA to extrapolate to all other regions in the Americas using the movement package in R<sup>51</sup>.

332 *European mobile phone data:* For Europe, we obtained mobile phone data (or call detail records,  
333 or CDRs) from three different countries where *Ae. albopictus* is present or has recently been  
334 detected: France<sup>43</sup>, Portugal<sup>52</sup>, and Spain<sup>43</sup>. CDR data contain the time at which a call was made  
335 or a text message was sent, the duration of the call, and the code of the cell in which  
336 communication started. The cell corresponds to an area covered by a specific mobile phone  
337 tower that serves a particular area. This means that the spatial resolution is restricted to the tower  
338 area, the specific location of each individual in the dataset cannot be ascertained. As our analysis  
339 was performed at the district level, all users' activity profiles were aggregated up to the district  
340 level, which is generally larger than cell tower areas. We thereby obtained a connectivity matrix  
341 that shows the connections made between each district *i* to each district *j* within each respective  
342 country.

343 For Portugal, data were available from over one million mobile phone users between April 2006  
344 and March 2007 (12 months). In Spain, CDRs were extracted from 1,034,430 users over three  
345 months between November 2007 and January 2008. In France we had the largest sample of  
346 5,695,974 users, collected between September 2007 and mid-October 2007 covering the entire  
347 country. Other aspects of the collection and processing methods have been described in detail

348 elsewhere<sup>23</sup>. We used the fitted models from Europe to extrapolate to all other regions in Europe,  
349 using the movement package in R<sup>51</sup>.

350 Human movement data for Asia: Mobility matrices for Asia are inferred from data from Chinese  
351 users of Baidu, the largest location-based service (LBS) in China. Baidu offers a large variety of  
352 apps and software for mobile devices and personal computers, mostly for online searching. We  
353 extracted GPS data from 23 April 2013 to 30 April 2014 (about 400 million users in China). The  
354 raw data was collected at the county level ( $n = 2,959$ ) and aggregated to the prefecture level (345  
355 prefectures). We then estimated daily flows of people between each pair of counties and  
356 aggregated this information per year. Movement is recorded in the Baidu data such that on each  
357 day if a user was observed at locations  $A \rightarrow B \rightarrow C$ , then  $A \rightarrow B$  and  $A \rightarrow C$  are counted which may  
358 produce biased population flow estimates. To explore potential bias in the data we compared the  
359 data derived from Baidu to a complete dataset of taxi-based GPS locations in the capital city of  
360 Hunan province, covering a one week period (full details below). The correlation of origin-to-  
361 destination flows in the city between the Baidu data and the complete taxi GPS data was very  
362 high ( $R^2 = 0.99$ ).

363 Baidu data validation: To verify the validity of the Baidu LBS data, we obtained a complete  
364 dataset of GPS locations for all taxis in Changsha city (capital of Hunan Province, population: 7  
365 million) in 2014. The location of each taxi is recorded for regulatory reasons using a GPS device  
366 in each taxi. The location is updated every 30 seconds. There were approximately 7,000 taxis in  
367 Changsha resulting in 20.16 million records ( $7000 * 24 * 60 * 2$ ) on a daily basis. The status of the  
368 cab was also recorded, such as the locations where passengers get on and off. These data are then  
369 used to extract the movements between the five districts in the main area of Changsha: Kaifu  
370 district, Furong district, Yuhua district, Tianxin district, and Yuelu district. For the purpose of

371 comparison, one week's data (April 4 to April 17, 2016) were extracted and analysed. The  
372 movements were normalized and then compared with the same week in 2014 from the Baidu  
373 LBS data. The correlation between the mobility estimates extracted from the Baidu LBS data and  
374 from the taxi's GPS data for Changsha city is presented in Extended Data Fig. 9. There is a high  
375 level of similarity between the two datasets, with a correlation coefficient of 0.99 ( $p=0.001$ ). We  
376 subsequently used the fitted models from China to extrapolate to other regions in Asia and  
377 Oceania again using the movement package in R51.

378 Human movement data for Africa: To calibrate the gravity and radiation models for Africa, we  
379 used aggregated and de-identified mobile phone-derived mobility estimates at the constituency  
380 level from Namibia between 1 October 2010 and 30 September 2011. These data represent the  
381 proportion of time that unique subscriber identity module (SIM) cards in each constituency  
382 spend in all other constituencies, as described in detail in Jones & Thornton (2000)<sup>53</sup>. We used  
383 this data set from Namibia because it was openly available and because it offered the best spatial  
384 and temporal resolution compared to census-derived data. We then used the fitted models to  
385 extrapolate to all other regions in Africa using the movement package in R51. Systematic  
386 surveys of cross-border human movements were not available at the time of the study and for the  
387 study regions.

388 It is possible that there are significant differences between regions in terms of mobility, but  
389 unfortunately no sufficiently widespread and well-resolved data source was available to test this.  
390 Our model captured the spread process of *Aedes* mosquitoes using a variety of human movement  
391 data, including both CDR data and commuting data. To assess the generalizability of our results  
392 we applied the model fitted to commuting data in the USA to the range expansion process  
393 observed in Europe. The predictive ability of this cross-continental validation indicates that the

394 mobility data used are sufficiently robust in the context of this study (Extended Data Fig. 8).  
395 However, we note there may be several limitations to using commuting data to infer vector  
396 introductions as they overly emphasize work-related movements. To test whether our model  
397 would perform well even in the absence of human movement data, we performed a cross  
398 validation that uses only distance and adjacency matrices which only marginally reduces  
399 predictability (Extended Data Fig. 12). Despite this, such data has indeed been used in the United  
400 States to successfully predict the long distance spread of infectious diseases. We are therefore  
401 confident that such data can be applied to predict both short and long distance spread in the  
402 USA<sup>54</sup>. Similarly, CDR data has been used to describe the spread of pathogens such as influenza  
403 in Europe<sup>23</sup>. As new data become available, our model is flexible enough to incorporate them  
404 and estimates of the predicted range expansion of *Ae. aegypti* and *Ae. albopictus* can be updated.  
405 There was also no suitable data available on cross border movements that could improve  
406 estimates of between-country spread (see section 2.4. for a sensitivity analysis).

## 407 2. Model fitting to data

### 408 2.1 Description of speed of dispersal:

409 To understand the past range expansion of both species and to provide basic summary statistics  
410 of the speed of dispersal over time in areas where sufficient observations were available, we use  
411 the methods of spread rate measurements employed by Tisseuil et al<sup>55</sup>. For each species and  
412 study area, the centroids of the spatial units where the species were observed were re-projected in  
413 a metric system (epsg 102003 in the US, and epsg 3035 in Europe) and the first date of detection  
414 in each centroid was interpolated on a 10 km resolution grid using thin plate spline regression  
415 (TPSR). The local slope of the surface was measured by a 3 x 3 moving windows filter, and the  
416 resulting friction surface (time / distance) was smoothed by an average 11 x 11 cell filter to

417 prevent local null frictions values. The local spread rate was then obtained by taking the inverse  
418 of the friction. This measure was computed within a mask, which was obtained by kernel density  
419 smoothing of the centroids of spatial units where the species were observed. We used the method  
420 of Berman and Diggle<sup>56</sup> to determine the optimal bandwidth for the US and EU invasions. In  
421 order to have a similar bandwidth for all masks, we used the maximum of the three estimated  
422 optimal bandwidths, which was found to be 73.2 km. A density threshold of 2.9 points per  
423 10,000 km<sup>2</sup> was chosen to delineate the mask, which was the maximum threshold value allowing  
424 the inclusions of all observation points in the mask in both the US and EU.

## 425 2.2. Mosquito environmental niche modelling

426 To predict the likely future distributions of both species independently (in years 2020, 2050 and  
427 2080), we first fitted species distribution models to data from the present day. This approach  
428 built on previous work<sup>4</sup> using the boosted regression tree (BRT) models fit to mosquito  
429 occurrence data (section 1.1.). BRTs combine strengths from regression trees and machine  
430 learning (gradient boosting) and are able to accommodate non-linear relationships to identify the  
431 environmental niche in which the environment is suitable for the species in question. After an  
432 initial regression tree is fitted and iteratively improved upon in a forward stepwise manner  
433 (boosting) by minimising the variation in the response variable not explained by the model  
434 at each iteration. This approach has been shown to simultaneously fit complex non-linear  
435 response functions efficiently while guarding against over-fitting.

436 We first developed a baseline scenario for the year 2015, using the global dataset of *Ae. aegypti*  
437 and *Ae. albopictus* occurrence (section 1.1)<sup>43,57</sup> and a set of environmental and socioeconomic  
438 predictors (section 1.2). In a BRT modelling framework pseudo-absences need to be generated to  
439 allow for discrimination between areas where the mosquitoes can persist, and to identify biases

440 in reporting<sup>58</sup>. We used the approach previously described in and applied by Kraemer et al<sup>4</sup> using  
441 background points from the Global Biodiversity Information Facility (GBIF) and the inverse of  
442 an *Aedes* temperature suitability mask<sup>45</sup> with equal ratio between presence and absence points  
443 and no threshold being applied. From that we constructed 100 sub-models to derive the mean  
444 prediction map and model-fitting uncertainty using the SEEG-SDM package in R<sup>59,60</sup>.

### 445 2.3. Human mobility modelling

446 Given the heterogeneous abundance of both species<sup>61</sup> as well as the low probability of their  
447 surviving slower and longer transits, the chance of a species being introduced following any  
448 single translocation event is low. Hence we used relatively long time steps (yearly) and  
449 generalized human movement models fitted to a variety of data sources to understand the spatial  
450 spread patterns of *Ae. aegypti* and *Ae. albopictus*.

451 We incorporated three distinct human movement models that act at different scales, since we are  
452 uncertain *a priori* which type of human movement will be most associated with mosquito spread.

453 We considered (i) a gravity model, (ii) a radiation model, (iii) an adjacency network model and  
454 (iv) un-transformed great-circle distance. Each of these models have been shown to be useful  
455 depending on the local context to infer regular daily commuting patterns, longer-term  
456 movements, and as general descriptions of human mobility<sup>24,62,63</sup>. First, the gravity model,

457 assumes that fluxes between two areas  $i$  and  $j$  are  $T_{i,j} = k \frac{N_i^\alpha N_j^\beta}{d_{i,j}^\gamma}$ , where  $N$  represents human

458 population size and  $d$  is great circle distance between two locations, and  $k$ ,  $\alpha$ ,  $\beta$ , and  $\gamma$  are  
459 parameters to be fit<sup>64,65</sup>. The gravity model emphasises the attractive power of large population

460 centres. Second, the radiation model assumes fluxes to be  $T_{i,j} = T_i \frac{N_i N_j}{(N_i + s_{i,j})(N_i + N_j + s_{i,j})}$ , where  $T_i$

461 is the number of individuals leaving area  $i$  and  $s_{ij}$  is the total population in the circle centered at

462  $i$  with radius  $d_{i,j}$  excluding the population of the two areas  $i$  and  $j$ . The radiation model  
463 considers not only distance and population sizes at origin and destination but also the cumulative  
464 population at a lesser distance from the origin than the destination<sup>24</sup>. Consequently, this model  
465 considers not only the origin and destination but also the landscape of ‘intervening opportunities’  
466 between them. Third, adjacency networks encode the number of district borders an individual  
467 would need to cross to move from one district to another. Thus, this metric reflects the  
468 neighbourhood effect. Finally, we computed the great-circle distance between each pair of  
469 locations and used that as a metric of mobility in and of itself<sup>32,66</sup>.

470 For each second Administrative unit (county/municipality) in the world, we determined the total  
471 human population size using gridded population estimates and calculated the great-circle  
472 distance between the centroids of each pair of districts within each continent<sup>67</sup>. Gravity and  
473 radiation model parameters were fitted by maximum likelihood methods to the empirical data  
474 described above using the movement R package<sup>51</sup>. National adjacency networks were computed  
475 using administrative boundary data from the GADM dataset (<http://www.gadm.org>). To account  
476 for neighbourhood effects of spread and for the potential importance of within-country and  
477 between-country movements, we constructed adjacency matrices that were disaggregated into  
478 three binary connectivity matrices with connectivity degrees of one (*i.e.*, districts share a border),  
479 two (*i.e.*, districts share a common neighbour), and three (*i.e.*, more than two degrees away).

#### 480 2.4. Mosquito spread modelling

481 Let  $x_i(t)$  be the *Aedes* population status of district  $i$  at time  $t$  (*i.e.*, a binary variable takes the  
482 value 1 if there were *Aedes* mosquitoes that time, and 0 otherwise). Given the nature of the  
483 dataset collected, we assumed that all data points represented detection of established  
484 populations and thus assumed continuous presence of the species for the first and last reported

485 occurrences. We used a standard logistic model to characterize the probability that some district  $j$   
486 will become occupied at time  $t$ :

$$\text{logit} \left( P(x_j(t) = 1 | x_j(t-1) = 0) \right) = \beta_0 + \sum_{k=1}^n \beta_k Y_{j,t}^{(k)}$$

487 where  $Y_{j,t}^{(k)}$  corresponds to the value of explanatory variable  $k$  in district  $j$  at time  $t$ . Explanatory  
488 variables included in this analysis were the predicted vector habitat suitability (*i.e.* suitability for  
489 establishment of an introduced vector, 2.1.) and connectivity between infested and non-infested  
490 districts (*i.e.* probability of introduction of a vector). Separate metrics of connectivity were  
491 defined for each human movement model (2.2.). From each human movement model, a  
492 connectivity matrix  $A_{ij}^{(k)}$  was calculated for each location  $i$  and  $j$ . A corresponding covariate for  
493 the occupation model was then computed to represent the global force of importation, exerted  
494 from all other infested districts to  $j$ :  $Y_{j,t}^{(k)} = \sum_i A_{ij}^{(k)} x_i(t-1)$ .

495 These models were re-fit in each successive year separately for the North American and  
496 European datasets, and for each vector species, using all available data up to that year. Model  
497 selection was done through backward selection using Akaike Information Criterion (AIC).<sup>68</sup> The  
498 fitted model was then evaluated prospectively over the next year by comparing predicted  
499 presence or absence with observations, thereby allowing us to evaluate and validate model  
500 performance over time. For model evaluation we considered all locations (*i.e.* 3,134 counties in  
501 the USA, 1,587 NUTS in Europe). This model evaluation was used to identify the best  
502 explanatory variables to include in the *Aedes* spread model. Model evaluation was performed  
503 using receiver operating characteristic curves (ROC curves) (Extended Data Fig. 7) and model  
504 accuracy was characterized comparing the predicted probabilities of first detection vs the

505 response (Extended Data Fig. 6). We calculated the probability of first detection  $p_w$  predicted by  
506 the model for each district-year that had not yet reported mosquitoes. We then partitioned  
507 district-years into eight groups with predicted probability in the range of 0-1%, 1-5%, 5-10%,  
508 10-15%, 15-20%, 20-25%, 25-35%, and 35-100%. For each group, we calculated the mean  
509 predicted probability and compared it with the proportion of district-years in the group in which  
510 range expansion was observed. Our model assumes that each mosquito species will persist in an  
511 area once detected, whilst there are some examples of incursions apparently having been  
512 successfully eradicated or died out. It is possible that this assumption could result in inflated  
513 predictions of the rate of spread, due to an overestimated number of source populations for each  
514 potential invasion event. However, it should be noted that this overestimate of the number of  
515 source populations would also be present in the training data, and would be at least partially  
516 absorbed into estimates of the probabilities of importation. Insufficient data were available to test  
517 or account for this potential bias, but based on additional experiments, we do not anticipate our  
518 estimates to greatly overpredict *Aedes* presence (see section: sensitivity analyses and sampling  
519 bias).

520 Cross-validation: To test whether the spread between countries is different to the spread within  
521 countries, we used the multi-country dataset from *Ae. albopictus* in Europe and varied the  
522 relative frequency of within- and between-country mobility by decreasing movement between  
523 countries by 20%, 50%, and 70%. The results were then compared with a baseline, in which  
524 predicted within-country movement is the same as between-country movement (Extended Data  
525 Fig. 11). We also performed sensitivity analyses to evaluate how a model including human  
526 movements compares to single variable models that have objective measurements such as great

527 circle distance and adjacency. A model that includes human movements only slightly increased  
528 predictive performance (Extended Data Fig. 12).

529 *Sensitivity analyses and sampling bias:* Surveillance efforts to detect *Ae. aegypti* and *Ae.*  
530 *albopictus* may vary in time and space due to gradual progressive improvements as a result of  
531 technology trapping technology, general expertise, or in response to specific events. Three types  
532 of possible changes in surveillance could bias the estimates of our spread model: (1) spatial  
533 expansion of surveillance system coverage to new areas; (2) intensification of sampling effort  
534 within areas where the surveillance system already operates; and (3) changes in sampling  
535 methods within areas where the surveillance system already operates that make it more or less  
536 likely to detect either *Ae. aegypti* or *Ae. albopictus*. To address each of these, we completed  
537 sensitivity analyses to understand how possible changes in surveillance may affect the inference  
538 about spread in the future.

539 Expansions of the surveillance system can be definitively distinguished from true known  
540 expansions of the vectors by comparing the state transitions of areas in longitudinal datasets,  
541 such as our *Ae. albopictus* dataset in Europe between the years of 2013 and 2017. Areas that first  
542 report absence of the species (often for multiple years) and later report presence are as close to a  
543 clear example of introduction as possible and give a reasonable estimate of the arrival date.  
544 Conversely, if an area's first report is presence of the species, the species' arrival date may have  
545 been estimated later than it truly occurred.

546 Firstly, the existence of such longitudinal records in the *Ae. albopictus* database in Europe is  
547 strong evidence that the distribution of the species is expanding, however to test if expanding  
548 surveillance efforts is a contributing factor to the observed rate of spread we compared our  
549 original model fit to the full *Ae. albopictus* in Europe dataset, as used in our main analysis

550 (model 1), with a model fit only to the data points that have strong evidence for a specific  
551 introduction date (i.e., report absence before presence; model 2). We tabulated data from *Ae.*  
552 *albopictus* in Europe where information was available whether there was ongoing surveillance  
553 prior to the reporting of the species (transition from absence to presence). Such data was  
554 available for 179 out of 600 observations between 2013 – 2018, a time period where 400 new  
555 regions reported the presence of the species making our sub-sample about 50% of all new  
556 invasions. This data was available at higher spatial resolution than the full *Ae. albopictus* dataset  
557 for Europe. 75% of these records are from locations of most recent spread in France and  
558 Germany. Finally, as model 2 was fit to data from a narrower date range we also consider a third  
559 model (model 3) which was fit to both occurrence and longitudinal data but only from the more  
560 recent date range (Extended Data Tab. 3). If expansion of surveillance efforts is a contributing  
561 factor to the observed rate of spread in the data, then we would expect Model 2 to predict a  
562 significantly lower rate of spread than Models 1 or 3 (our null hypothesis).

563 Each of these models were fit to the above datasets, then used to simulate *Ae. albopictus* spread  
564 from a common baseline (based on occurrence and longitudinal data at the end of 2012) for five  
565 years between 2013 and 2017 as described previously. The predicted total number of new  
566 districts infested of this period was calculated and is shown in Extended Data Tab. 4. Note that  
567 comparison of goodness of fit metrics for these models was not possible since the models were  
568 fit to different datasets.

569 Contrary to the expectation that more precise dates of invasion would lead to conclusions of  
570 slower rates of spread, this sensitivity exercise found that restricting the model to just areas  
571 where the date of introduction is known significantly increases the predicted rate of spread. Thus,  
572 this exercise rejects our above null hypothesis. This effect was also independent of the time

573 period of the fitting data (similar results for Model 1 and Model 3). These results suggest that it  
574 is more likely that true spread of *Ae. albopictus* is outpacing expansion of mosquito surveillance,  
575 and if longitudinal surveillance was in place everywhere, the observed rates of spread would be  
576 greater.

577 We therefore believe that the currently implemented model is a conservative estimate of spread  
578 of these species that is not highly affected by changes in spatial coverage of surveillance systems  
579 and provides the most robust estimates of spread over these time periods given the available data.  
580 Given the limited number of years of data available to fit Model 2, we believe that Model 1  
581 provides the most reliable estimates of future spread.

582 Intensification in sampling effort and technological advancements in collection methods may  
583 affect the probability of detection of a species in earlier in their invasion process vs today. Here  
584 we test both hypotheses through inclusion of different terms in our spread model regression and  
585 compare such models to the null of no changes in surveillance intensity over time (as currently  
586 implemented in our main analysis). To represent increases or decreases in surveillance over time,  
587 we include the spline-smoothed year of detection as a variable in the regression analysis. To  
588 represent step changes in surveillance efforts in response to specific events we include a factor  
589 variable; either before the 2003 peak in West Nile Virus cases in the USA, or after 2003 (only  
590 for models in USA). Internal cross validation was then used to compare the predictive  
591 performance of these three models with evaluation on three-year-lookahead holdout sets, subject  
592 to a minimum of 10 consecutive years of data to fit the models. Model predictive performance  
593 was then compared using deviance from observed values in the holdout set.

594 This showed that for all species in all continents, the inclusion of a temporal (Year) term reduced  
595 predictive accuracy (increased deviance). This was the case for both gradual change over time

596 (s(Year)) and for breakpoint changes in response to specific events (Year > 2003). As a result,  
597 we conclude that there is no evidence for temporal changes in sampling effort in any of the  
598 datasets concerned and therefore do not include such terms in our final predictions (Extended  
599 Data Tab. 5).

600 Finally, there is a possibility that changes in general vector surveillance strategies could have led  
601 to changes that affected the probability of detection of one species more than the other. Such  
602 differential biases could undermine our inter-species spread rate comparison. One key period of  
603 concern is around the 2003 West Nile Virus (WNV) outbreak in the US where vector  
604 surveillance may have prioritized trapping in more rural environments to optimize detection of  
605 various *Culex* species. Such a focus on rural environments may have led to relative increases in  
606 sampling intensity of *Ae. albopictus* and relative reductions in sampling intensities for *Ae.*  
607 *aegypti*.

608 To test this hypothesis, we follow a similar approach to the above analysis, where covariates for  
609 “before” and “after” the 2003 WNV outbreak are included in the USA spread model for each  
610 species. If the above hypothesis is true, such terms should i) have larger “after” values than  
611 “before” values in the *Ae. albopictus* model and vice versa in the *Ae. aegypti* model, and ii)  
612 improve model prediction accuracy.

613 The best fits from the *Ae. aegypti* and *Ae. albopictus* spread models in the USA show that  
614 detection of *Ae. aegypti* marginally increased relative to *Ae. albopictus* (positive model  
615 coefficients for post-2003 term in *Ae. aegypti*, negative in *Ae. albopictus*) (Extended Data Tab.  
616 6). However, as previously stated, inclusion of such changes in surveillance quality over time  
617 reduces the model predictive performance (increase in deviance for both species) and therefore  
618 may not provide a better time period to mirror the spread of the species in the United States.

## 619 2.5. Classifying the ranges of each mosquito species and incorporating uncertainty

620 Current reported distributions of *Ae. aegypti* and *Ae. albopictus* are unlikely to be fully  
621 representative of their actual distributions because of logistical and financial constraints on  
622 vector surveillance.<sup>37</sup> Therefore we used the following method to estimate the current-day global  
623 distribution (realised niche) of each mosquito species by comparing environmental suitability  
624 maps with occurrence data. We extracted the predicted environmental suitability value at each of  
625 the locations where the mosquito species has been reported, and the value of environmental  
626 suitability that encompassed 90% of these reported locations was chosen as the range threshold.  
627 Every value above or equal to this threshold was defined as within the range of the mosquito  
628 species (Extended Data Fig. 13). This approach assumes that the 10% of occurrences outside of  
629 the predicted range represent temporary introductions that do not persist longer than one year and  
630 are not representative of the long-term distribution of the species. As there is uncertainty in what  
631 proportion of the data are representative of these transient identifications (given that the majority  
632 of the data are cross-sectional not longitudinal), we undertook a sensitivity analysis that varied  
633 this threshold from 85% to 95%, thereby creating 96 different possible range maps that represent  
634 different realisations of the current distribution of each species. In doing so, we capture locations  
635 that have the conditions for mosquito presence and where there is potential for onward spread.  
636 We did not include international shipping as a contributor to infrequent long-distance  
637 importation events between continents since both species are already well established on each  
638 continent and therefore new occurrences are more likely to be driven by intra-continental  
639 importation pressure.

### 640 3. Future projections

#### 641 3.1. Projecting environmental and socioeconomic covariates

642 We used 17 GCMs to estimate 30 arc-sec images for monthly mean climate data. Extended Data  
643 Table 7 provides the designation, origin, references and number of replicate runs for each model.  
644 The procedures are described in detail in MarkSim documentation<sup>65</sup>. For each GCM the baseline  
645 monthly climate was derived from the historic runs for temperatures and rainfall, the monthly  
646 means were calculated for each GCM for the years 2000 to 2095, and the difference ‘delta’ for  
647 each month was calculated by subtracting the specific GCM baseline. The deltas were  
648 interpolated from the native GCM pixel (Extended Data Tab. 7) to a one degree by one degree  
649 pixel for the globe. The data were pattern scaled to WorldClim 1.03<sup>64</sup> for each one degree pixel,  
650 RCP, and month. For each variant a fourth order polynomial regression was fitted over the 96  
651 years of data and through the origin at 1985 (1985 being the mean midpoint of the data used in  
652 the WorldClim construction) to calculate one output per model per year per scenario.

653 Humidity data were estimated directly at the 30 arc-sec level from dewpoint calculated by the  
654 tabular method of Linacre<sup>69</sup> and the mean temperature. To fully propagate the variation between  
655 the climate models through our predictions we used the outputs of 17 GCM, for all 3 years, and 3  
656 scenarios.

657 Global temperature estimates were converted into temperature suitability for mosquito  
658 population persistence (separate metrics for each vector species), hereafter referred to as  
659 temperature suitability, using temperature-based mathematical models from Riahi et al<sup>44</sup> and  
660 Fujino et al<sup>45</sup>. These show the effects of diurnal and seasonal changes in temperatures on the  
661 generation time of the mosquito and its resultant effects on the persistence of a population.

662 As a highly anthropophilic mosquito species, the future distribution of the *Aedes* is likely to  
663 depend critically on both environmental and human socioeconomic factors that modify the  
664 availability of its habitat<sup>8</sup>. To incorporate these features, we also modelled the continued process  
665 of global urbanisation until 2080 using a probabilistic machine learning algorithm based on the  
666 work of Linard et al<sup>48</sup>. Here we use urban growth rates predicted by the United Nations as a  
667 predictor variable<sup>49</sup> as well as a range of other covariates as previously described in van Vuuren  
668 et al<sup>48</sup>.

### 669 3.2. Projecting future niche of *Ae. aegypti* and *Ae. albopictus*

670 Although niche shifts might occur over long time-periods, the future effects remains unclear for  
671 *Ae. aegypti* and *Ae. albopictus* since their expansion from their native range<sup>70</sup>. Therefore, we  
672 assume niche conservatism, implying that the mosquitoes tend to establish and survive under  
673 similar environmental conditions in native and invaded ranges in the future<sup>4,71,72</sup>.

674 Our final aim was to produce 18 maps predicting *Ae. aegypti* and *Ae. albopictus* suitability in the  
675 years 2020, 2050 and 2080 under three different emissions scenarios (RCPs). Each of these 18  
676 maps were composed of 100 ensemble predictions that randomly sampled (with replacement) the  
677 following aspects of the analysis:

- 678 1. The fitted *Aedes* BRT model (from a choice of 100 BRT models fitted to 2015 data)
- 679 2. The predicted temperature suitability for *Aedes* survival (from a choice of 17 GCMs)
- 680 3. The predicted minimum precipitation (from a choice of 17 GCMs)
- 681 4. The predicted relative humidity (from a choice of 17 GCMs)
- 682 5. The predicted minimum precipitation (from a choice of 17 GCMs)
- 683 6. The predicted geographic expansion via land from the spread models (section 3.3).

684 This approach sought to fully propagate the uncertainty in the climate, *Aedes* temperature  
685 suitability and *Aedes* models through to the final prediction. These 100 predictions were then  
686 summarised by mean and 95% credible intervals to give the final prediction for each year RCP  
687 combination. Uncertainties are shown in all maps along the X-axes.

688 Our baseline map modelling is different from previously published maps in so far that it uses  
689 only projectable environmental and socio-demographic variables and does not use the Enhanced  
690 Vegetation Index (EVI), as the EVI is a direct empirical measure of the Earth's current  
691 greenness<sup>4</sup>. To minimise potential reduction in the predictive ability of the model by omitting  
692 this covariate, we include precipitation and relative humidity as predictors for suitability for  
693 green vegetation growth in both the present day and future models.

### 694 3.3. Projecting mosquito spread

695 To derive yearly model-based estimates of the possible expansion of both species by 2080 we  
696 forward-simulated the geographic spread model based on the equation in 2.4. To account for the  
697 spatio-temporal dependence in first detection probabilities (each district's probability is a  
698 function of every other district that was infested the year before), we run 1,000 simulations  
699 forward in time. Within each simulation we estimate the probability of infestation to each district  
700 that had yet to detect the species. We then drew a Bernoulli random variable with that probability  
701 of '1' (i.e., invasion) and imputed those results for each potential detection. Using these imputed  
702 invasions as well as all districts that had previously been infested, we repeat the estimation of  
703 range expansion for the next year. This process is repeated up to the desired forecast horizon.  
704 This represents a single simulation. It is important to note that we did not allow for the situation  
705 where an already infested district will 'lose' its infection status (*i.e.*, if  $x_i(t - 1) = 1$  for district

706  $i$ , we force  $x_i(t) = 1$ ). We then combine the results of the 1,000 simulations to identify which  
707 districts were most likely to have a positive species presence at any point.

#### 708 3.4. Calculating population at risk and area expansion

709 To classify areas as at risk or not at risk of *Ae. aegypti* and *Ae. albopictus* a threshold was  
710 defined for the continuous *Aedes* suitability maps by the value that maximised sensitivity and  
711 specificity when classifying the occurrence and background data using the 2015 map. This value  
712 was found to be 0.47 and 0.51 for *Ae. aegypti* and *Ae. albopictus* respectively. Any pixel with a  
713 predicted suitability value above that was considered at risk and the same threshold was applied  
714 to each time point and scenario to calculate the population and area at risk in each global region.  
715 The final maps for 2020, 2050, 2080 are then overlaid with contemporary estimates of human  
716 populations at 5 km resolution and extracted the relevant population at risk was estimated using  
717 the raster package in R. We paired the climatic scenarios based on Shared Socioeconomic  
718 Pathways (SSPs) that were defined by O'Neill *et al.* in 2014<sup>73</sup>. They represent reference  
719 pathways that describe plausible alternate trends in the evolution of society and ecosystems over  
720 a century, in the absence of climate change or climate policies. SSPs are predicated on possible  
721 outcomes that would make it more or less difficult to respond to climate change challenges. Each  
722 SSP consists of quantified population and Gross Domestic Product (GDP) trajectories, serving as  
723 the starting points for various organisations to model these factors and to provide projections for  
724 demographic and economic development variables. The Integrated Assessment Modelling  
725 Consortium (IAMC) made available certain peer-reviewed projections via the International  
726 Institute for Applied Systems Analysis (IIASA, <http://www.iiasa.ac.at>), whereby the SSP  
727 storylines were converted into population and GDP projections for 195 countries<sup>74</sup> for every  
728 decade between the years 2010 and 2100.



730 **References**

- 731 1. Nsoesie, E. O. *et al.* Global distribution and environmental suitability for chikungunya  
732 virus, 1952 to 2015. *Eurosurveillance* **21**, pii=30234 (2015).
- 733 2. Messina, J. P. *et al.* Mapping global environmental suitability for Zika virus. *Elife* **5**,  
734 e15272 (2016).
- 735 3. Bhatt, S. *et al.* The global distribution and burden of dengue. *Nature* **496**, 504–7 (2013).
- 736 4. Kraemer, M. U. G. *et al.* The global distribution of the arbovirus vectors *Aedes aegypti*  
737 and *Ae. albopictus*. *Elife* **4**, e08347 (2015).
- 738 5. Lessler, J. *et al.* Assessing the global threat from Zika virus. *Science* **353**, aaf8160 (2016).
- 739 6. Faria, N. R. *et al.* Epidemic establishment and cryptic transmission of Zika virus in Brazil  
740 and the Americas. *Nature* **546**, 406–10 (2017).
- 741 7. Grubaugh, N. D., Ladner, J. T., Kraemer, M. U. G., Dudas, G. & Tan, A. L. Genomic  
742 epidemiology reveals multiple introductions of Zika virus into the United States. *Nature*  
743 **546**, 401–5 (2017).
- 744 8. Messina, J. P. *et al.* The many projected futures of dengue. *Nat. Rev. Microbiol.* **13**, 230–9  
745 (2015).
- 746 9. Kraemer, M. U. G. *et al.* Progress and challenges in infectious disease cartography.  
747 *Trends Parasitol.* **32**, 19–29 (2016).
- 748 10. Powell, J. R. Mosquitoes on the move. *Science* **354**, 971–972 (2016).
- 749 11. Powell, J. R. & Tabachnick, W. J. History of domestication and spread of *Aedes aegypti* -  
750 a review. *Mem. Inst. Oswaldo Cruz* **108 Suppl**, 11–7 (2013).
- 751 12. Scott, T. W. *et al.* Longitudinal Studies of *Aedes aegypti* (Diptera: Culicidae) in  
752 Thailand and Puerto Rico: Blood Feeding Frequency. *J. Med. Entomol.* **37**, 89–101 (2000).
- 753 13. Guerra, C. A. *et al.* A global assembly of adult female mosquito mark-release-recapture  
754 data to inform the control of mosquito-borne pathogens. *Parasites and Vectors* **7**, 276  
755 (2014).
- 756 14. Hawley, W. A., Pumpuni, C. B., Brady, R. H. & Craig, G. B. Overwintering survival of  
757 *Aedes albopictus* (Diptera, Culicidae) eggs in Indiana. *J. Med. Entomol.* **26**, 122–129  
758 (1989).
- 759 15. Maynard, A. J. *et al.* Tiger on the prowl: Invasion history and spatio-temporal genetic  
760 structure of the Asian tiger mosquito *Aedes albopictus* (Skuse 1894) in the Indo-Pacific.  
761 *PLoS Negl Trop Dis* **11**, e (2017).
- 762 16. Benedict, M. Q., Levine, R. S., Hawley, W. a & Lounibos, L. P. Spread of the tiger: global  
763 risk of invasion by the mosquito *Aedes albopictus*. *Vector borne zoonotic Dis.* **7**, 76–85  
764 (2007).
- 765 17. Armbruster, P. A. Review Photoperiodic Diapause and the Establishment of *Aedes*  
766 *albopictus* (Diptera: Culicidae) in North America. *J. Med. Entomol.* **53**, 1013–1023 (2016).
- 767 18. Vega-rua, A. *et al.* High Efficiency of Temperate *Aedes albopictus* to Transmit

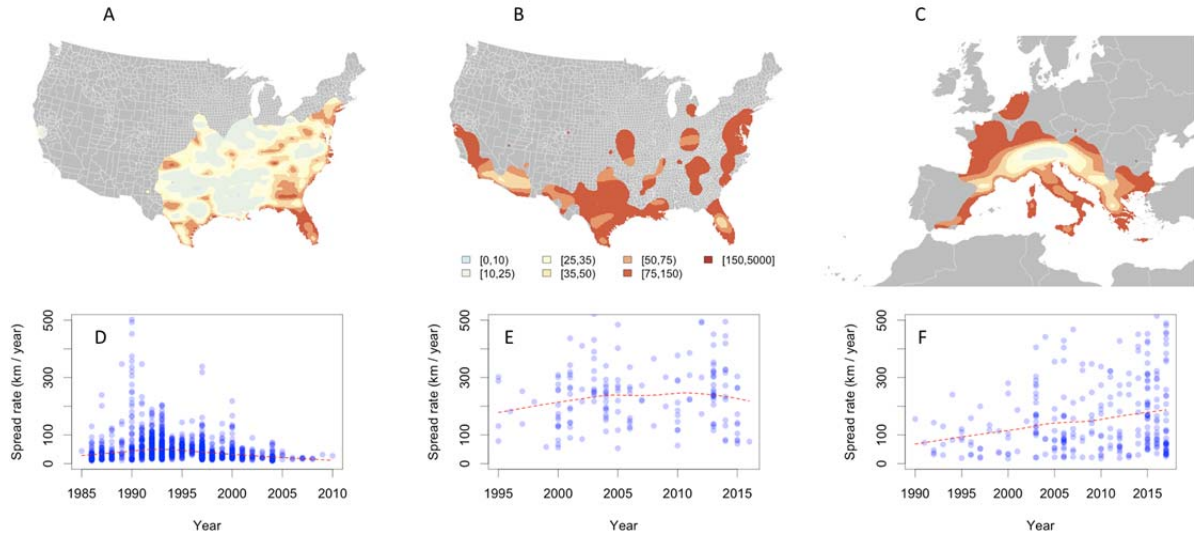
- 768 Chikungunya and Dengue Viruses in the Southeast of France. *PLoS One* **8**, e59716 (2013).
- 769 19. Gloria-soria, A. *et al.* Global genetic diversity of *Aedes aegypti*. *Mol. Ecol.* **25**, 5377–  
770 5395 (2016).
- 771 20. Padilla, D. K., Chotkowski, M. A. & Buchan, L. A. J. Predicting the Spread of Zebra  
772 Mussels (*Dreissena polymorpha*) to Inland Waters Using Boater Movement Patterns. *Glob.*  
773 *Ecol. Biogeogr. Lett.* **5**, 353–359 (1996).
- 774 21. Roche, B. *et al.* The Spread of *Aedes albopictus* in Metropolitan France: Contribution of  
775 Environmental Drivers and Human Activities and Predictions for a Near Future. *PLoS*  
776 *One* **10**, e0125600 (2015).
- 777 22. Moore, C. G., Medicine, V., Sciences, B. & State, C. Using Geographic Information  
778 Systems to Analyze the Distribution and Abundance of *Aedes aegypti* in Africa : The  
779 Potential Role of Human Travel in Determining the Intensity of Mosquito Infestation. *Int.*  
780 *J. Appl. Geospatial Res.* **4**, 9–38 (2013).
- 781 23. Tizzoni, M. *et al.* On the use of human mobility proxies for modeling epidemics. *PLoS*  
782 *Comput. Biol.* **10**, e1003716 (2014).
- 783 24. Simini, F., González, M. C., Maritan, A. & Barabási, A.-L. A universal model for mobility  
784 and migration patterns. *Nature* **484**, 96–100 (2012).
- 785 25. Simini, F., Maritan, A. & Néda, Z. Human mobility in a continuum approach. *PLoS One* **8**,  
786 e60069 (2013).
- 787 26. Canali, M., Rivas-Morales, S., Beutels, P. & Venturelli, C. The Cost of Arbovirus Disease  
788 Prevention in Europe: Area-Wide Integrated Control of Tiger Mosquito, *Aedes albopictus*,  
789 in Emilia-Romagna, Northern Italy. *Int. J. Environ. Res. Public Health* **14**, 444 (2017).
- 790 27. Leishnam, P. T., Lounibos, L. P., O’Meara, G. F. & Juliano, S. A. Interpopulation  
791 divergence in competitive interactions of the mosquito *Aedes albopictus*. *Ecology* **90**,  
792 2405–13 (2009).
- 793 28. Camara, D. C. P. *et al.* Seasonal differences in density but similar competitive impact of  
794 *Ae. albopictus* (Skuse) and *Aedes aegypti* (L.) in Rio de Janeiro, Brazil. *PLoS One* **11**,  
795 e0157120 (2016).
- 796 29. Lounibos, L. P. *et al.* Does temperature affect the outcome of larval competition between  
797 *Aedes aegypti* and *Aedes albopictus*? *J. Vector Ecol.* **27**, 86–95 (2002).
- 798 30. Prinzing, A., Durka, W., Klotz, S. & Brandl, R. Geographic variability of ecological  
799 niches of plant species: Are competition and stress relevant? *Ecography (Cop.)*. **25**, 721–  
800 729 (2002).
- 801 31. Soberón, J. Grinnellian and Eltonian niches and geographic distributions of species. *Ecol.*  
802 *Lett.* **10**, 1115–1123 (2007).
- 803 32. Kraemer, M. U. G. *et al.* Big city, small world: density, contact rates, and transmission of  
804 dengue across Pakistan. *J. R. Soc. Interface* **12**, 20150468 (2015).
- 805 33. Kraemer, M. U. G. *et al.* Spread of yellow fever virus outbreak in Angola and the  
806 Democratic Republic of the Congo 2015–16: a modelling study. *Lancet Infect. Dis.* **17**,

- 807 330–338 (2017).
- 808 34. Perkins, T. A., Siraj, A. S., Ruktanonchai, C. W., Kraemer, M. U. G. & Tatem, A. J.  
809 Model-based projections of Zika virus infections in childbearing women in the Americas.  
810 *Nat. Microbiol.* **16126**, (2016).
- 811 35. Bogoch, I. I. *et al.* Potential for Zika virus introduction and transmission in resource  
812 limited countries in Africa and Asia-Pacific. *Lancet Infect. Dis.* **16**, 1237–45 (2016).
- 813 36. Bogoch, I. I. *et al.* Anticipating the international spread of Zika virus from Brazil. *Lancet*  
814 **387**, 335–336 (2016).
- 815 37. Schaffner, F. *et al.* Development of guidelines for the surveillance of invasive mosquitoes  
816 in Europe. *Parasit. Vectors* **6**, 209 (2013).
- 817 38. Moore, C. G. & Mitchell, C. J. *Aedes albopictus* in the United States: ten-year presence  
818 and public health implications. *Emerg. Infect. Dis.* **3**, 329–34 (1997).
- 819 39. Flacio, E., Engeler, L., Tonolla, M., Lüthy, P. & Patocchi, N. Strategies of a thirteen year  
820 surveillance programme on *Aedes albopictus* (*Stegomyia albopicta*) in southern  
821 Switzerland. *Parasites and Vectors* **8**, (2015).
- 822 40. Collantes, F. *et al.* Review of ten-years presence of *Aedes albopictus* in Spain 2004 –  
823 2014 : known distribution and public health concerns. *Parasit. Vectors* **8**, (2015).
- 824 41. Eritja, R., Palmer, J. R. B., Roiz, D., Sanpera-calbet, I. & Bartumeus, F. Direct Evidence  
825 of Adult *Aedes albopictus* Dispersal by Car. *Sci. Rep.* **7**, 14399 (2017).
- 826 42. Salje, H. *et al.* Dengue diversity across spatial and temporal scales: Local structure and the  
827 effect of host population size. *Science* **355**, 1302–1306 (2017).
- 828 43. Kraemer, M. U. G. *et al.* The global compendium of *Aedes aegypti* and *Ae. albopictus*  
829 occurrence. *Sci. Data* **2**, 150035 (2015).
- 830 44. Brady, O. J. *et al.* Global temperature constraints on *Aedes aegypti* and *Ae. albopictus*  
831 persistence and competence for dengue virus transmission. *Parasit. Vectors* **7**, 338 (2014).
- 832 45. Brady, O. J. *et al.* Modelling adult *Aedes aegypti* and *Aedes albopictus* survival at  
833 different temperatures in laboratory and field settings. *Parasit. Vectors* **6**, 351 (2013).
- 834 46. IPCC. *Climate Change 2013: the physical science basis: contribution of working group I*  
835 *to the Fifth Assessment Report on The Intergovernmental Panel on Climate Change, IPCC*  
836 *Fifth Assessment Report: Climate Change 2013 (AR5)*. (Cambridge University Press,  
837 2013).
- 838 47. UNFCCC (United Nations Framework Convention on Climate Change). Adoption of the  
839 Paris Agreement. *21st Conf. Parties* (2015).
- 840 48. Linard, C., Tatem, A. J. & Gilbert, M. Modelling spatial patterns of urban growth in  
841 Africa. *Appl. Geogr.* **44**, 23–32 (2013).
- 842 49. United Nations Population Division. *World Urbanization Prospects: The 2014 Revision*.  
843 (United Nations, 2014).
- 844 50. Hahn, M. B. *et al.* Reported Distribution of *Aedes* (*Stegomyia*) *aegypti* and *Aedes*

- 845 (Stegomyia) albopictus in the United States, 1995-2016 (Diptera: Culicidae). *J. Med.*  
846 *Entomol.* 1–7 (2016). doi:10.1093/jme/tjw072
- 847 51. Golding, N., Schofield, A. & Kraemer, M. U. G. Movement: Functions for the analysis of  
848 movement data in disease modelling and mapping. *R Packag. version 0.2* (2015).
- 849 52. Osório, H. *et al.* Detection of the Invasive Mosquito Species *Aedes* (Stegomyia)  
850 albopictus (Diptera: Culicidae) in Portugal. *Int. J. Environ. Res. Public Heal.* 2018, Vol.  
851 15, Page 820 **15**, 820 (2018).
- 852 53. Ruktanonchai, N. W. *et al.* Identifying Malaria Transmission Foci for Elimination Using  
853 Human Mobility Data. *PLOS Comput. Biol.* **12**, e1004846 (2016).
- 854 54. Viboud, C. *et al.* Synchrony, waves, and spatial hierarchies in the spread of influenza.  
855 *Science* **312**, 447–51 (2006).
- 856 55. Tisseuil, C. *et al.* Evaluating methods to quantify spatial variation in the velocity of  
857 biological invasions. *Ecography (Cop.)*. **39**, 409–418 (2015).
- 858 56. Berman, M. & Diggle, P. Estimating weighted integrals of the second-order intensity of a  
859 spatial point process. *J. R. Stat. Soc. Ser. B* **51**, 81–92 (1989).
- 860 57. Kraemer, M. U. G. *et al.* Data from: the global compendium of *Aedes aegypti* and *Ae.*  
861 albopictus occurrence. *Dryad Digit. Repository* (2015). doi:dx.doi.org/10.5061/dryad.47v3c
- 862 58. Phillips, S. J. *et al.* Sample selection bias and presence-only distribution model:  
863 implications for background and pseudo-absence data. *Ecol. Appl.* **19**, 181–97 (2009).
- 864 59. R Core Team. R: A language and environment for computing. Vienna, Austria. *R Found.*  
865 *Stat. Comput.* (2016).
- 866 60. Golding, N. Streamlined functions for species distribution modelling in the seeg research  
867 group. *R Packag. version 0.1-3* (2014).
- 868 61. Perkins, T. A., Scott, T. W., Le Menach, A. & Smith, D. L. Heterogeneity, mixing, and  
869 the spatial scales of mosquito-borne Ppathogen transmission. *PLoS Comput. Biol.* **9**,  
870 e1003327 (2013).
- 871 62. Brockmann, D. & Helbing, D. The hidden geometry of complex, network-driven  
872 contagion phenomena. *Science* **342**, 1337–42 (2013).
- 873 63. Jongejans, E. *et al.* A unifying gravity framework for dispersal. *Theor. Ecol.* **8**, 207–223  
874 (2015).
- 875 64. Wesolowski, A., O’Meara, W. P., Eagle, N., Tatem, A. J. & Buckee, C. O. Evaluating  
876 Spatial Interaction Models for Regional Mobility in Sub-Saharan Africa. *PLOS Comput.*  
877 *Biol.* **11**, e1004267 (2015).
- 878 65. Wesolowski, A. *et al.* Commentary: Containing the Ebola outbreak – the potential and  
879 challenge of mobile network data. *PLOS Curr. Outbreaks* **Sep 29**, (2014).
- 880 66. Tatem, A. J., Hemelaar, J., Gray, R. R. & Salemi, M. Spatial accessibility and the spread  
881 of HIV-1 subtypes and recombinants. *AIDS* **26**, 2351–60 (2012).
- 882 67. WorldPop project. WorldPop. Available at: <http://worldpop.org.uk/>.

- 883 68. Hastie, T. J. & Tibshirani, R. J. *Generalized additive models*. (CRC Press, 1990).
- 884 69. Linacre, E. T. A simple formula for estimating evaporation rates in various climates, using  
885 temperature data alone. *Agric. Meteorol.* **18**, 409–424 (1977).
- 886 70. Medley, K. A. Niche shifts during the global invasion of the Asian tiger mosquito, *Aedes*  
887 *albopictus* Skuse (Culicidae), revealed by reciprocal distribution models. *Glob. Ecol.*  
888 *Biogeogr.* **19**, 122–33 (2010).
- 889 71. Wiens, J. J. & Graham, C. H. Niche conservatism: integrating evolution, ecology, and  
890 conservation biology. *Annu. Rev. Ecol. Evol. Syst.* **36**, 519–39 (2005).
- 891 72. Petitpierre, B. *et al.* Climatic Niche Shifts Are Rare Among Terrestrial Plant Invaders.  
892 *Science* **338**, 1344–8 (2012).
- 893 73. O'Neill, B. C. *et al.* A new scenario framework for climate change research : the concept of  
894 shared socioeconomic pathways. *Clim. Change* **122**, 387–400 (2014).
- 895 74. Kc, S. & Lutz, W. Demographic scenarios by age, sex and education. *Popul. Environ.* **35**,  
896 243–260 (2014).
- 897 75. Elith, J., Leathwick, J. R. & Hastie, T. A working guide to boosted regression trees. *J.*  
898 *Anim. Ecol.* **77**, 802–13 (2008).
- 899 76. Rochlin, I., Ninivaggi, D. V, Hutchinson, M. L. & Farajollahi, A. Climate Change and  
900 Range Expansion of the Asian Tiger Mosquito ( *Aedes albopictus* ) in Northeastern USA :  
901 Implications for Public Health Practitioners. *PLoS One* **8**, e60874 (2013).
- 902 77. Ogden, N. H., Milka, R., Caminade, C. & Gachon, P. Recent and projected future climatic  
903 suitability of North America for the Asian tiger mosquito *Aedes albopictus*. *Parasit.*  
904 *Vectors* **7**, in press (2014).
- 905 78. Butterworth, M. K., Morin, C. W. & Comrie, A. C. An Analysis of the Potential Impact of  
906 Climate Change on Dengue Transmission in the Southeastern United States. *Environ.*  
907 *Health Perspect.* **125**, 579–585 (2017).
- 908

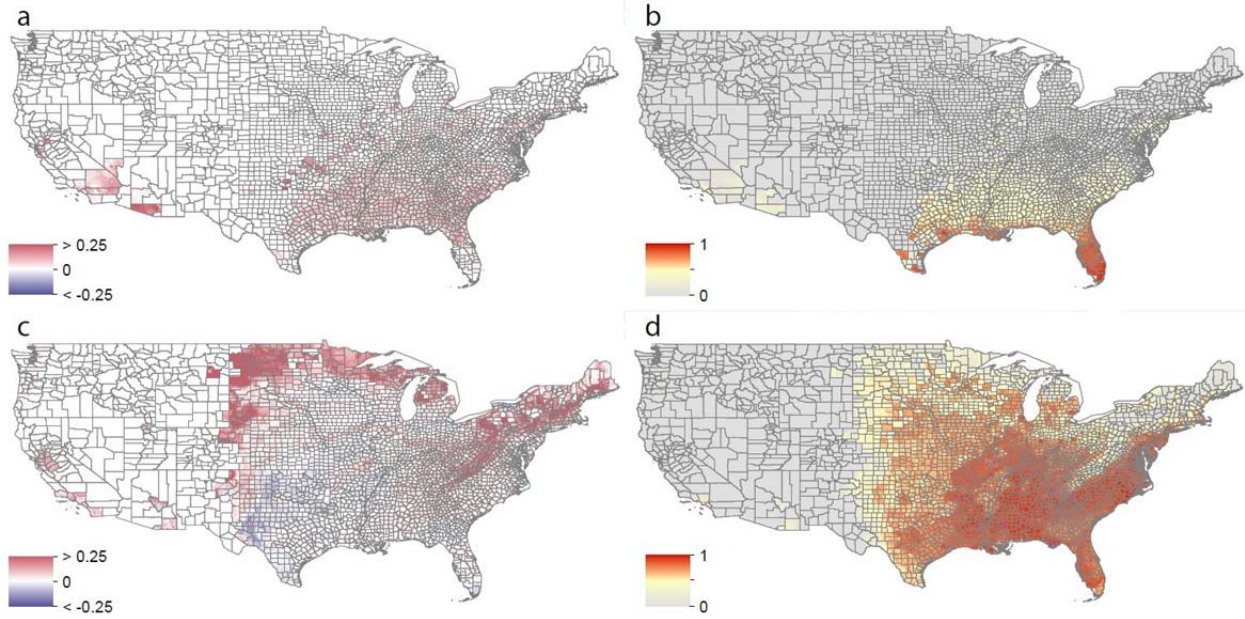
909 Figures



910

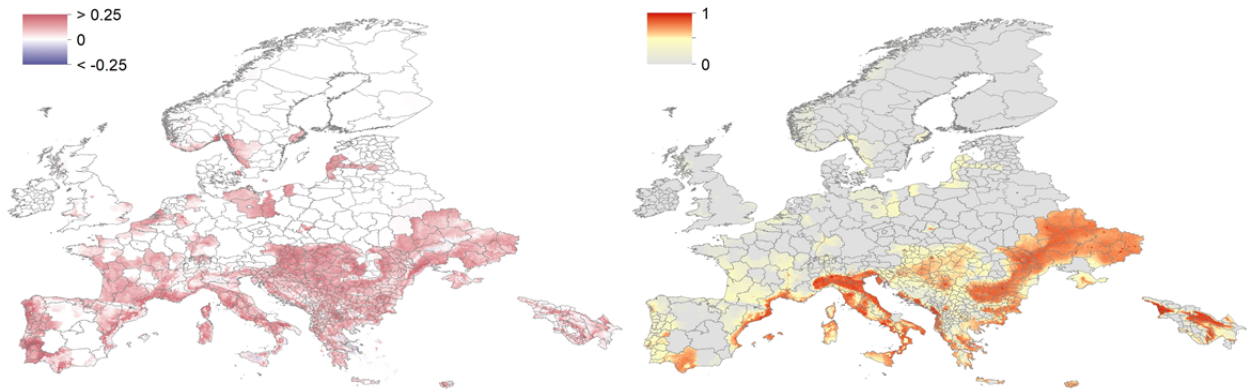
911 **Fig. 1:** Reconstruction of *Ae. albopictus* and *Ae. aegypti* spread in the United States (a and b respectively),  
912 and *Ae. albopictus* in Europe (c). Estimates of speed of spread in km/year are based on thin spline  
913 regression on mosquito observations since their earliest detection in each continent. Red indicates fast  
914 dispersal (km/year) whereas yellow and white indicate slower spread (km/year) velocity (see legend  
915 below panel b). Areas highlighted in grey have no reported mosquito presence. Panels d – f summarise  
916 the speed of dispersal of *Ae. albopictus* and *Ae. aegypti* spread in the United States (d, e) and of *Ae.*  
917 *albopictus* in Europe (f) starting from their date of first detection until 2017. The red line indicates the  
918 average velocity per year across all districts using the thin spline regression model.

919



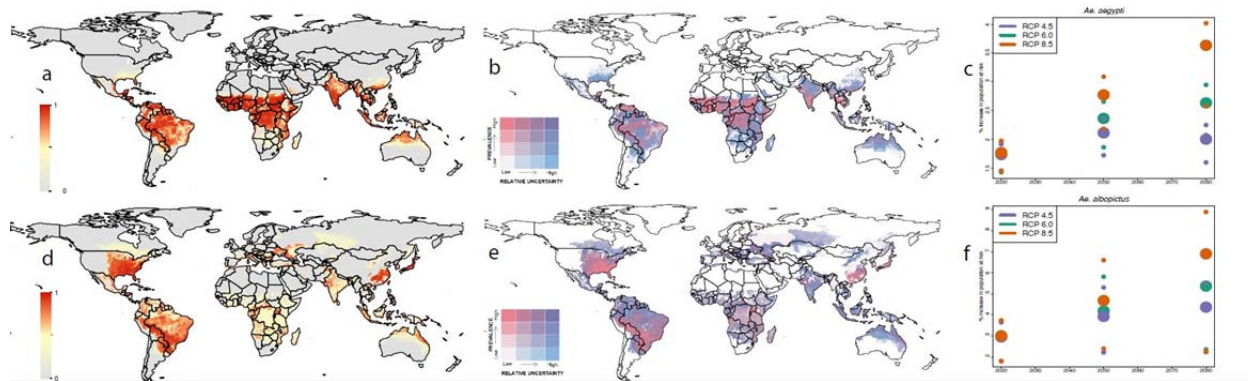
920

921 **Fig. 2:** Predicted future spread of *Aedes aegypti* and *Aedes albopictus* in the United States, estimated  
 922 using human-mobility metrics and ecological determinants fitted to past occurrence data. Panel A shows  
 923 the forecasted change in the distribution of *Ae. aegypti* between 2020 and 2050 using the medium climatic  
 924 scenario Representative Concentration Pathways 6.0 at the United States county level ranging from -0.25  
 925 (blue) to 0.25 (red). Red indicates expansion and dark blue contraction of the *Aedes* range distribution  
 926 between 2020 and 2050. Panel b shows the predicted suitability of presence of *Ae. aegypti* in 2050.  
 927 Pixels with no predicted suitability are coloured in grey. Panels c and d show the corresponding  
 928 results for *Ae. albopictus*.



929

930 **Fig. 3:** Predicted future spread of *Aedes albopictus* in Europe. Panel a shows the expansion (red) and  
 931 contraction (blue) of *Ae. albopictus* between 2020 and 2050 under the medium climate scenario RCP6.0  
 932 with emissions peaking in 2080. Panel b shows the predicted distribution of *Ae. albopictus*. Panel b  
 933 shows the predicted suitability of presence of *Ae. albopictus* in 2050. Pixels with no predicted  
 934 suitability are coloured in grey.



935

936 **Fig. 4:** Predicted global geographic distribution of *Ae. aegypti* (a) and *Ae. albopictus* (c) in 2050 under the  
 937 medium climatic scenario RCP6.0 and uncertainty for *Ae. aegypti* (b) and *Ae. albopictus* (e). Predicted  
 938 suitability of *Ae. aegypti* quantile cutoff points were 0.24, 0.66, 0.88. Relative uncertainty was  
 939 computed as the ratio of the 95% uncertainty intervals and predicted *Ae. aegypti* suitability for each  
 940 pixel. Cutoff points for uncertainty were 0.08, 0.18, 0.31. The lowest quantile of predicted suitability  
 941 is shown in white, and the highest in dark pink. The lowest quantile for uncertainty is white and the  
 942 highest is blue. The colours overlap such that areas coloured purple have both high predicted  
 943 suitability of *Ae. aegypti* and high relative uncertainty. Pixels with no predicted suitability are  
 944 coloured in grey. Panel c show the corresponding results for *Ae. albopictus*. Predicted suitability of  
 945 *Ae. albopictus* quantile cutoff points were 0.13, 0.41, 0.70. Cutoff points for uncertainty for *Ae.*  
 946 *albopictus* were 0.16, 0.36, 0.53. The global population predicted to live in areas suitable for *Ae.*  
 947 *aegypti* (b) and *Ae. albopictus* (c) under the conservative (RCP4.5), medium (RCP6.0), and worst-  
 948 case scenario (RCP8.5) using the binary cutoff values of suitability of 0.46 and 0.51 for both species  
 949 respectively.

950

951• *Acknowledgements:* We want to thank Sarah Ray for editorial review. MUGK acknowledges funding  
952 from the Society in Science, The Branco Weiss Fellowship, administered by the ETH Zurich. MUGK  
953 also acknowledges funding from the Training Grant from the National Institute of Child Health and  
954 Human Development (T32HD040128). MUGK and SIH acknowledge funding from the International  
955 Research Consortium on Dengue Risk Assessment Management and Surveillance (IDAMS; European  
956 Commission 7<sup>th</sup> Framework Programme #21893). SIH received a grant from the Research for Health in  
957 Humanitarian Crises (R2HC) Programme, managed by ELRHA (#13468) which also supported MUGK  
958 and NG. The R2HC programme aims to improve health outcomes by strengthening the evidence base for  
959 public health interventions in humanitarian crises. The £8 million R2HC programme is funded equally by  
960 the Wellcome Trust and Department of International Development (DFiD), with Enhancing Learning and  
961 Research for Humanitarian Assistance (ELRHA) overseeing the programme's execution and management.  
962 SIH was also funded by a Senior Research Fellowship from the Wellcome Trust (#95066) and grants  
963 from the Bill & Melinda Gates Foundation (OPP1106023, OPP1093011, OPP1132415 and OPP1159934).  
964 This study was made possible by the support of the American people through the United States Agency  
965 for International Development Emerging Pandemic Threats Program-2 PREDICT-2 (Cooperative  
966 Agreement number AID-OAA-A-14-00102), which also supported MUGK. JSB is supported by the  
967 National Library of Medicine of the National Institutes of Health (R01LM010812, R01LM011965),  
968 which also supports MUGK. DLS is funded by the National Institutes of Health and National Institute of  
969 Allergy and Infectious Diseases (#U10AI089674). HHN was funded by the European Commission  
970 through the European Research Council Advanced Investigator Grant 'Momentum' 324247. LL received  
971 funding from the French Government's Investissement d'Avenir program, Laboratoire d'Excellence  
972 Integrative Biology of Emerging Infectious Diseases (grant ANR-10-LABX-62-IBEID), the French  
973 Agence Nationale de la Recherche (grant ANR-16-CE35-0004), the City of Paris Emergence(s)  
974 programme in Biomedical Research, and the European Union's Horizon 2020 research and innovation  
975 programme under ZikaPLAN grant agreement No 734584. NG is supported by a University of Melbourne  
976 McKenzie fellowship. WVB, GH, and FS acknowledge funding from VBORNET and VectorNet, an  
977 ECDC and EFSA funded project (#ECDC/09/018 and OC/EFSA/AHAW/2013/02), and thank all  
978 contributing VBORNET/VectorNet experts for data sharing. TWS, RCR, and LL received funding from  
979 the National Institutes of Health Program Project grant (#P01 AI098670). XL is supported by the Natural  
980 Science Foundation of China (71522014, 71725001, 71690233 and 71731009).

981 *Author Contributions:* All contributions are listed in order of authorship. Designed the experiments:  
982 MUGK, RCR, OJB, SIH, NG; Provided data: SL, XL, PJ, LB, EW, AJT, GEC, RGC, WVB, GH, FS,  
983 CGM, HY, QL; Analyzed the data: MUGK, RCR, OJB, JPM, MG; Interpreted the results: MUGK, RCR,  
984 OJB, JPM, MG, DY, DB, TAP, HHN, DLS, LL, SC, NRF, OGP, TWS, GRWW, SIH, NG; Edited the  
985 manuscript: JPM, LBM, NDW, SS, GRWW, SIH; Wrote the manuscript: MUGK, OJB, OGP, SIH, NG;  
986 All authors read and approved the content of the manuscript.

987 *Conflicts of Interest:* We declare no competing financial interests.

988 Reprints and permissions information is available at [www.nature.com/reprints](http://www.nature.com/reprints)

989 Correspondence and requests for materials should be addressed to [moritz.kraemer@zoo.ox.ac.uk](mailto:moritz.kraemer@zoo.ox.ac.uk)